Performance Evaluation of Exact Cone-Beam Algorithms for the Long-Object Problem in Spiral Computed Tomography

K. Sourbelle[1], H. Kudo[2], G. Lauritsch[3], K.C. Tam[4], M. Defrise[5] and F. Noo[6]
[1]Institute of Medical Physics, University of Erlangen, 91054 Erlangen, Germany
[2]Institute of Information Sciences and Electronics, University of Tsukuba, Tsukuba 305-8573, Japan
[3]Siemens Medical Solutions, P.O. Box 3260, 91050 Erlangen, Germany
[4]Siemens Corporate Research, Inc., Princeton, NJ 08540, USA
[5]Division of Nuclear Medicine, AZ-VUB, Free University of Brussels, 1090 Brussels, Belgium
[6]Institute of Electricity Montefiore, University of Liège, 4000 Liège, Belgium

I. Introduction

Spiral Computed Tomography (CT) with area detectors is of increasing interest for scanning large volumes in a short time and achieving isotropic resolution. When the cone-angle is large, exact reconstruction algorithms are needed which go beyond approximate solutions.

A major problem of spiral cone-beam CT is the so-called long-object problem, which concerns the exact reconstruction of a region-of-interest (ROI) of a long object using projection data of a pure spiral scan covering the ROI and its immediate vicinity only. This problem has been recently solved with different approaches: the Virtual Circle method [1], the Zero Boundary method [2], and the Local ROI technique [3]. Although all these methods are theoretically justified, they have different approaches and therefore some differences in numerical behavior and in effectiveness are expected.

The purpose of this study is to evaluate the performances of these algorithms regarding image quality and practicability. Here, we concentrate on Filtered-Backprojection-type (FBP) algorithms. A comparison between Radon- and FBP-based algorithms for the Local ROI method can be found in [4]. Image quality is determined on the basis of image artifacts, spatial resolution and noise properties. For practicability, the computing time as well as the overscan range required for the ROI reconstruction (i.e. the z-extension of the spiral below and above the ROI) are compared.

II. Description Of The Methods

The reconstruction of a short-object from axially truncated projections can be performed with an exact (or quasi-exact) 3D Filtered Backprojection (FBP) approach, as proposed in [5][6]. The method is based on the generalization of Grangeat's formula for calculating the Radon data and requires the cone-beam projections to be measured in some region B on the detector which is bounded by the projection of the upper and of the lower turn of the spiral. A straightforward implementation of the filtering step is the 4-step algorithm, which consists in performing some line integral derivatives on the cone-beam projection, backprojecting them on a virtual detector (which is large enough to cover the cone-beam projection of the whole object) and applying a final derivative filter. Alternatively, the filtering step can be carried out by convolution with an 1D ramp filter plus some boundary correction term involving only data at the boundaries of the region B [5][6] (these boundaries will be referred below as the mask boundaries). The 4-step algorithm is the basis of the Local ROI method whereas the 1D ramp filter approach is the basis of the Virtual Circle and of the Zero Boundary methods.

A. *The Virtual Circle Method (VC)*

One solution to the long-object problem is to add two supplementary circle scans at the bottom and at the top of the ROI [7]. However, this is not practical for medical imaging. It can be shown that the particular projection data of the circle scans needed for the reconstruction of the ROI can be synthesized from the data of the spiral scan. Therefore a real measurement of the circle scans is not necessary and the synthesized data are regarded as virtual data.

B. *The Zero Boundary Method (ZB)*

Since only the data on the boundaries of the region B cause troubles in the long-object problem, the Zero Boundary method treats them separately. The image to be reconstructed is expressed as the sum of two partial images. The first image can be reconstructed such that its cone-beam projections are equal to the data on the mask boundaries, exploiting the property that each point in the field-of-view belongs to one and only one PI-line. The second image can be reconstructed from the projections with zeroed mask boundaries, using a standard 3D FBP with ramp filtering and cone-beam backprojection.

C. *The Local ROI Method (LR)*

In the Local ROI technique [3], the Radon derivative data are grouped on ϕ-planes (meridian planes) containing the z-axis. The Radon derivative data on different ϕ-planes are computed for different portions of the object, which are called local ROI's. Each local ROI is defined by the parallel projection of the spiral scan path onto the corresponding ϕ-plane, so that the contributing cone beams are not contaminated by object information outside the local ROI. A (global) ROI consisting of the intersection of all local ROI's can be reconstructed without interference from the parts of the object outside the ROI. The Local ROI method was formulated as a Radon-based algorithm [8], as well as an FBP-based 4-step algorithm [9][10].

III. Simulation Experiments

Image quality is evaluated with simulated projection data. The scanner geometry is based on standard parameters of medical scanners: the radius of the focus path is 57 cm and the detector is at the distance 43.5 cm from the z-axis. We take 1056 projections per rotation. We choose a table feed value of 12.8 cm per turn, which corresponds to a full cone-angle of 7.2°. For this large angle, approximate algorithms usually do not perform well any more.

Different phantoms are used for this study: a 3D anthropomorphic Head Phantom [11] for the investigation of artifacts, simulated ideal delta points for the evaluation of spatial resolution, and a homogeneous water sphere phantom of 20 cm diameter for the study of noise properties. The simulations are done for a flat detector with square pixels of dimensions $(0.88\ \text{mm})^2$, which corresponds to a square pixel size of $(0.5\ \text{mm})^2$ at the center of rotation. For the Head phantom and the water sphere, the simulated detector has 512×256 pixels.

The VC and the ZB methods have been implemented as originally published in [1] and [2], respectively. The filtering of the 4-step in the LR method has been implemented with the help of the linogram method [12], yielding an improvement in efficiency and accuracy, compared to the original published algorithm [10].

IV. Evaluation Of Image Quality

A. Visual Image Impression and Artifacts

The reconstructions of the Head Phantom for the three methods are shown in Fig. 1. The results of the reconstruction of the whole object are compared with a ROI reconstruction. For the whole object reconstruction, the spiral consists of 2.97 turns covering a z-range of [-19 cm, 19 cm]; the ROI reconstruction is obtained from projections of 2 turns covering the range [-12.8 cm, 12.8 cm]. The reconstructed volumes consist of 512^3 voxels of dimensions $(0.5\ \text{mm})^3$.

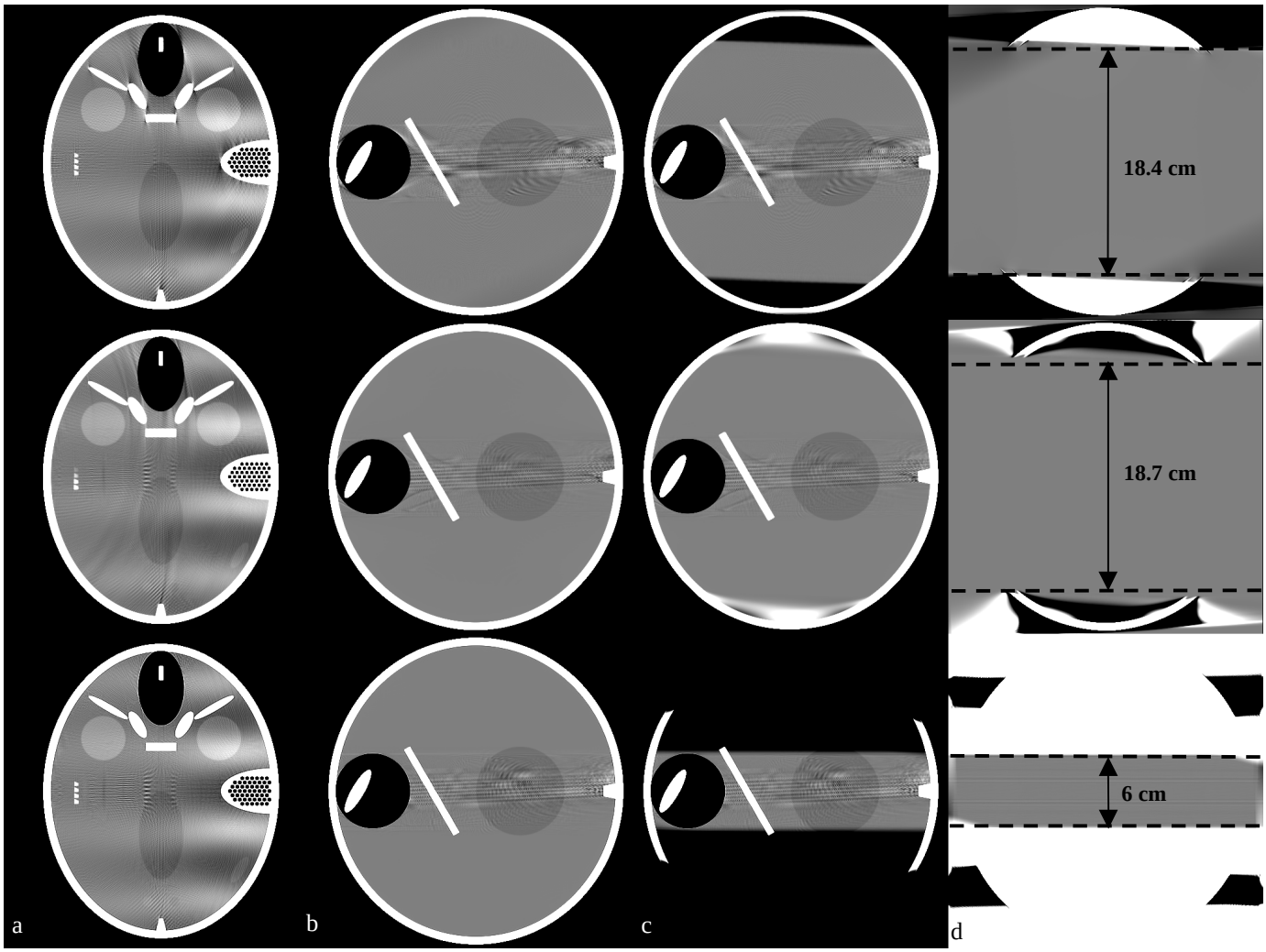

Fig. 1: Reconstruction of the 3D Head phantom for the three different algorithms. First row: VC. Second row: ZB. Third row: LR. a) xy-plane at z=0 b) yz-plane at x=0 with reconstruction of the whole object, c) yz-plane at x=0 with ROI reconstruction, d) difference between b) and c) - Window settings: a) to c) (C50, W80) d) (C0,W20)

The images are of good quality for all algorithms. The different objects of the phantom are well represented despite the relatively large cone-angle. The ROI reconstruction does not bring additional artifacts, which proves that the methods for short- and long-object reconstructions are equivalent.

A noticeable artifact is the wave in the axial slice, which comes from the small air bubbles of the right inner ear and is present for all methods. At the moment, we do not understand the origin of this artifact.

The ZB method presents some small artifacts in the region of the frontal sinus, which is probably due to a resolution mismatch between the 2 partial images. Some small artifacts are also to be seen in the VC method. None of these artifacts are present for the LR method, but we can notice undershooting around some of the high contrast objects. This undershooting is probably related to the calculation of the derivative filters in the 4-step algorithm.

B. Spatial Resolution

We simulate an ideal delta point at the origin of the coordinate system (x=y=z=0) and reconstruct the 3D Point Spread Function (PSF) for each algorithm. The reconstruction is performed with a voxel size of $(0.02\ \text{mm})^3$.

The in-plane Modulation Transfer Function (MTF) is obtained from the 3D PSF in the slice z=0 by averaging the radial profiles over all angles and performing a subsequent Hankel transform (see Fig. 2).

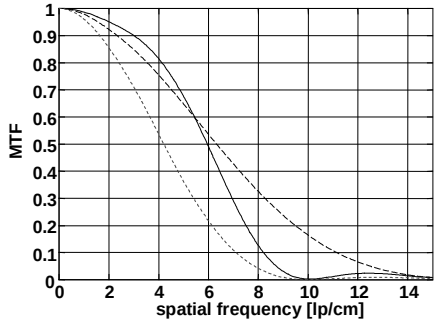

Fig. 2: In-plane MTF for the LR (solid line), the VC (dashed line) and the ZB method (dotted line). The Nyquist frequency is 10 lp/cm.

The VC and ZB methods should have a similar behavior since they both apply a ramp filter. The difference noted here comes from the difference in the current implementations since the ZB method uses a Hamming window in comparison to the Shepp-Logan window used for the VC method. This also explains why the MTF of the VC method extends beyond the Nyquist frequency, thus causing a risk of aliasing. The ZB and LR algorithms cut off at the Nyquist frequency, while LR yields better frequency representations than ZB.

To characterize in-plane resolution, we choose the 5% value (ρ_5) of the in-plane MTF value. The values can be found in Table 1. A Nyquist frequency of 10 lp/cm is expected from the horizontal detector aperture.

To determine axial resolution, we calculate the Slice Sensitivity Profile (SSP) which is derived from the 3D PSF by taking the profile along z at the position x=y=0 (see Fig. 3). Axial resolution is characterized by the value of the Full Width at Half Maximum (FWHM) of the SSP (see Table 1).

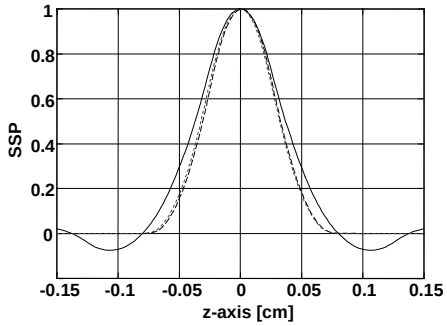

Fig. 3: SSP for the LR (solid line), the VC (dashed line) and the ZB method (dotted line)

The VC and the ZB methods have an identical SSP since they are almost equivalent in the axial direction (no filtering). We obtain a FWHM of about 1.27 collimated slices. The axial resolution of the LR method is less good (about 1.5 collimated slice widths). Moreover, we notice the undershooting already seen in Fig.1.

Note that the PSF's of the algorithms are shift-variant due to the magnification effect of the cone-beam backprojection.

Table 1
In-plane / axial spatial resolutions and noise level
for the three methods

	LR	VC	ZB
ρ_5 [lp/cm]	8.7	12.5	7.9
$FWHM_{SSP}$ [cm]	0.074	0.063	0.064
σ_{Noise} [HU]	9.7	14.2	6.7

C. Noise Properties

In order to model real quanta noise, we add attenuation dependent randomized gaussian noise to the original intensity projections before taking the logarithm. To compare the noise performances of the algorithms, we simulate and reconstruct a sphere of diameter 20 cm of constant density. As a measure of noise, the standard deviation of pixel gray values is evaluated in an area of (2 cm × 2 cm) centered in the slice z=0.

The amount of noise is strongly related to spatial resolution (see Table 1). Thus, the VC method with its superior spatial resolution shows more noise than the other methods.

V. PRACTICABILITY

A. Overscan

As shown in Fig. 1.c, the three methods require different overscan ranges to reconstruct a ROI. This overscan depends on the transaxial radius of the ROI (see Fig. 4). For objects of small radius (radius < 0.5 of the scan path radius), the LR method needs a larger overscan than the other two methods. The minimum spiral length required for exact ROI

reconstruction is still unclear and is subject to further investigations.

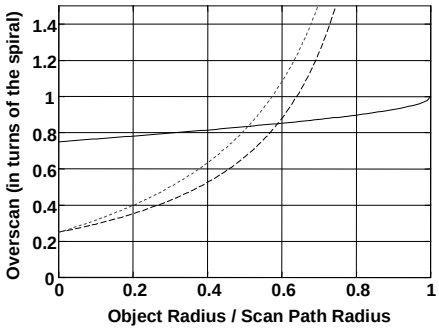

Fig. 4: Overscan expressed in terms of turns of the spiral as a function of the radius of the object: LR (solid line), VC (dashed line) and ZB method (dotted line).

For the Head Phantom (maximal object radius = 12 cm), we find overscan values of 4.6 cm, 5.2 cm and 10 cm along the z-axis for the VC, ZB and LR methods, respectively, which corresponds to a minimal theoretical ROI size of 16.4 cm, 15.2 cm and 5.6 cm. Since the object is not a cylinder but an ellipsoid, the real size of the ROI's might be larger. Note that the ROI that can be exactly reconstructed usually is not cylindrical but has slanted edges with respect to the xy-plane.

B. Reconstruction Time

The reconstruction time of the three non-optimized implementations presented here for the reconstruction of the ROI of the Head phantom are given in Table 2. The times have been obtained on a Pentium 450MHz with 512 MB memory.

The reconstruction times are quite long in comparison to standard 2D CT reconstruction algorithms. The VC and ZB methods are much faster than the LR method because of the simple filtering step. The ZB method requires more effort due to the separate treatment of the projection data on the mask boundaries consisting of 3D re- and backprojection, but on the other hand the backprojection is much faster since the size of the filtered detector is smaller.

Table 2
Reconstruction time in hours for the ROI reconstruction of Fig. 1.c.

LR	VC	ZB
100	45	51

C. Data Handling

The VC and LR methods are quite attractive since they are of real FBP-type. The ZB method in comparison requires many steps for creating the 2 partial images and therefore also a lot of disk memory to save the temporary results. On the other hand, the FBP for VC and LR has to be done on a virtual detector which is much larger than the original detector depending on the reconstructed ROI size, whereas the FBP of ZB can be done on the original detector. However it is possible to perform multi ROI reconstructions as proposed in [1].

VI. CONCLUSION

All three algorithms achieve an image quality good enough to match the requirements of clinical applications. However, the long computation times are prohibitive for any usage beyond research applications.

In terms of image quality, all algorithms investigated here are comparable. It turns out that the three algorithms have a good stability and that the main factor affecting the image quality of the reconstructions is the filter design. In the current implementations, the images of the LR method show less artifacts, while the VC algorithm yields the higher spatial resolution. In terms of practicability, the VC method is superior to the ZB and LR methods. For most clinical applications, it requires fewer projections and less computing time to reconstruct a given ROI. The overscan strongly depends on the size of the objects; while the LR method is not competitive for small objects (e.g. head), the amount of overscan is comparable for larger objects like thorax or abdomen.

VII. ACKNOWLEDGMENT

This work was supported in part by the Bavarian Center of Excellence for Medical Imaging FORBILD.

VIII. REFERENCES

[1] H. Kudo, F. Noo, M. Defrise, "Quasi-exact filtered backprojection algorithm for long-object problem in helical cone-beam tomography", *IEEE Trans. Med. Imag.*, vol. 19, Sept 2000, pp. 902-921

[2] M. Defrise, F. Noo, H. Kudo, "A solution to the long-object problem in helical cone-beam tomography", *Phys. Med. Biol.*, vol. 45, pp. 623-644, March 2000

[3] F. Sauer, S. Samarasekera, K.C. Tam, "Practical cone-beam image reconstruction using local regions-of-interest", U.S. patent 6,009,142, December 28, 1999

[4] K. Sourbelle, G. Lauritsch, K.C. Tam, F. Noo, W.A. Kalender, "Performance evaluation of local ROI algorithms for exact ROI reconstruction in spiral cone-beam computed tomography", *Proc. of IEEE Med. Imag. Conf*, Lyon, 2000

[5] H. Kudo, F. Noo, M. Defrise, "Cone-beam filtered-backprojection algorithm for truncated helical data", *Phys. Med. Biol.*, vol. 43, pp. 2885-2909, 1998

[6] K.C. Tam, B. Ladendorf, F. Sauer, G. Lauritsch, A. Steinmetz, "Backprojection spiral scan region-of-interest cone-beam CT", *Proc. Of SPIE Med. Imag.*, vol 3661, pp 433-441, 1999

[7] K.C. Tam, "Helical and circle scan region of interest computerized tomography", *US. Patent 5,463,666*, October 31, 1995.

[8] S. Schaller, F. Noo, F. Sauer, K.C. Tam, G. Lauritsch, T. Flohr, "Exact Radon rebinning algorithm for the long object problem in helical cone-beam CT", *IEEE Trans. Med. Imag.*, vol. 19, May 2000

[9] K.C. Tam, "Exact local regions-of-interest reconstruction in spiral cone-beam filtered-backprojection CT: theory", *Proc. of SPIE Med. Imag.*, vol. 3979, pp. 506-519, 2000

[10] G. Lauritsch, K.C. Tam, K. Sourbelle, S. Schaller, "Exact local regions-of-interest reconstruction in spiral cone-beam filtered-backprojection CT: numerical implementation and first image results", *Proc. of SPIE Med. Imag.*, vol. 3979, pp. 520-532, 2000

[11] http://www.imp.uni-erlangen.de/forbild

[12] C. Jacobson, "Fourier methods in 3D-reconstruction from cone-beam data", *PhD Thesis*, Linköping University, Sweden, 1996